Effect of Rapid Thermal Annealing of CIGS Thin Film as an Absorber Layer

J.R. Ray[1], M.S. Desai[1], C.J. Panchal[1,*], Bharati Rehani[2], P.K. Mehta[3]

[1] *Applied Physics Department, Faculty of Technology and Engineering, The M.S. University of Baroda, Vadodara-390001 Gujarat, India*

[2] *Metallurgical and Materials Engineering Department, Faculty of Technology and Engineering, The M.S. University of Baroda, Vadodara-390001 Gujarat, India*

[3] *Physics Department, Faculty of Science, The M.S. University of Baroda, Vadodara-390001 Gujarat, India*

The influence of rapid post-deposition thermal annealing (500 °C for 2 minutes) on the CIGS thin films of different thicknesses (0.4 to 1.0 µm) has been investigated. The deposition of CIGS is carried out using the flash evaporation at the substrate temperature of 250 °C. The as-grown and annealed CIGS is characterized by XRD, SEM, EDS, TEM, optical transmission, reflection, and electrical measurements. Lowering the thickness of CIGS absorber shows the remarkable influence on crystal structure, surface morphology, and composition of the overall film. Further improvement was observed by the rapid annealing process. Cu-rich composition was observed for annealed CIGS thin film having a thickness below 0.6 µm, while for 1.0 µm thickness the composition is slightly Cu-poor and the compactly packed faceted grains observed. Optical band gap near to 1.05 eV and the electrical resistivity in the order of 10^4 Ω·cm shows its future use as an absorber layer for CIGS solar cell. Furthermore, an attempt of making CIGS / CdS hetero-structure shows ideal behavior of the Schottky hetero-structure with the ideality factor of 1.5.

Keywords: CIGS thin film, Rapid thermal annealing, XRD, SEM, EDS, TEM.

PACS numbers: 81.40.Ef, 61.05.cp, 68.37.Hk, 68.37.Lp

1. INRODUCTION

Among the various types of thin film based solar cells available in the market, CIGS thin film solar cells have been considered to be the most promising alternatives to crystalline silicon solar cells because of their high solar to electricity conversion efficiency, reliability, and stability [1]. However, current industrial approach for the fabrication of CIGS solar cell are based on vacuum processes such as co-evaporation [2, 3], sputtering techniques [4], sequential evaporation and selenization [5], closed space vapor transport [6] and spray pyrolsis [7]. Even though these methods result in highly efficient CIGS solar cells, they generally require initially high capital investment as well as maintenance capital expense [1, 8]. Many research groups show the effective performance of the CIGS based solar cell, by depositing the CIGS layer using somewhat less expensive deposition methods like thermal evaporation [9], flash evaporation [10], screen printing of nano particles [11], etc. reducing the thickness of absorber layer is the another approach for reducing the overall cost of the solar cell [12, 13, 14]. Commercial CIGS thin film solar cells fabricated by co-evaporation having a 2 to 3 micron thickness of absorber layer (active layer). Decreasing the thickness of CIGS layer further is especially important for indium and gallium metals as the supply of these metals may become an issue if the production of large scale CIGS thin-film solar cells modules is continuing. Decreasing the thickness of CIGS layer below 1 micron could lead to reduction in the production cost, with no, or only minor, loss in performance. However we should note that there is a possibility of the shunting of the device, as observed by T. Negami et al., for the absorber thickness less then 0.5 µm [15].

Nevertheless, further improvements in the growth and composition of thinned CIGS layer can control the device degradation. CIGS is a self-doped (intrinsically doped) material, which means that, when the compound is formed, it automatically becomes either p- or n-type, depending upon the elemental composition present in the bulk and the surface of the film. The primary intrinsic defects, which are also called native defects, include copper vacancies (V_{Cu}), copper-on-indium of gallium ($Cu_{In/Ga}$) antisites, indium/gallium-on-copper antisites (In/Ga_{Cu}), and selenium vacancies (V_{Se}). The former two produce acceptor type defects, whereas the latter two give rise to donor-type defects. Yuuki Umeno et al. [16] studied the Se to metal flux ratio affects the grain growth of CIGS thin films. In wide band-gap devices (1.4 eV) large grains of CIGS thin films grew as the Se to metal flux ratio was 51. On the other hand, small grains formed for a Se to metal flux ratio of 118. The annealing of CIGS films at high temperature (> 450 °C) in inert atmosphere results the inter-diffusion of In and Ga in segregated CIS and CGS phases, resulting in a homogeneous CIGS phase [17]. Note that the Cu content lower than the 25 at. % required for the stoichiometric compound, especially to avoid the presence of Cu_xSe segregations, which are usually present when depositing the stoichiometric or near-stoichiometric compound on large areas [18, 19] and it is the most detrimental defect for lowering the solar cell performance. While thinning the absorber layer one has to check the various properties like growth, crystal structure, surface morphology, electrical, optical, etc., for obtaining the optimum performance of solar cell. In the present work all these properties of CIGS thin films are studied by varying the CIGS film thickness from

---

* cjpanchal_msu@yahoo.com

1.0 μm to 0.4 μm with and without annealing. CIGS thin films grown at 250 °C and rapidly annealed at 500 °C in the rapid thermal annealing (RTA) furnace for 2 min in Argon (Ar) environment.

2. EXPERIMENTAL DETAILS

The $CuIn_{1-x}Ga_xSe_2 : x = 0.3$ (CIGS) (5 % excess selenium) bulk compound was evaporated by the flash evaporation technique. The compound preparation, characterization and the film deposition details are discussed elsewhere [20, 21]. Different thicknesses (0.4-1.0 μm) of CIGS thin films are deposited at 250 °C substrate temperature. The thermal annealing of the CIGS thin films was carried out using RTA furnace at 500 ºC for 2 minutes. Fig. 1 shows the timing diagram for temperature control of the RTA furnace.
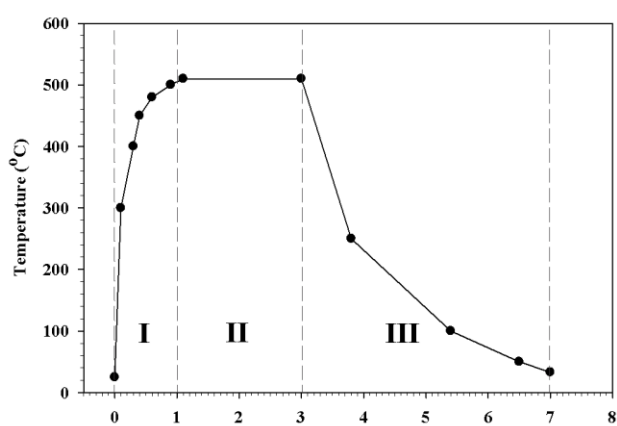

Fig. 1 – Timing diagram for the RTA process for CIGS thin films divided in three regions: (I) ramp up period, (II) controlled temperature period, and (III) ramp down period

The thickness is measured using the quartz crystal monitor. The structural characterization of the CIGS thin films was carried out using an X-ray diffractometer (XRD), D8 advance, bruker-make, in 2θ range of 20º-80º, at a scan-rate of $0.05°\,s^{-1}$, using CuKα radiation. Surface and chemical analysis of a particular film area and/or a particles present in the film is analyzed by JSM-7001F scanning electron microscopy (SEM) with EDS analysis facility. TEM was carried out using the JEOL, JEM 2100F having accelerating voltage of 80 to 200 kV, a resolution of 0.14 nm lattice, and magnification is × 50 to 1,500,000. The optical transmittance and reflectance measurements have been carried out with unpolarized light source (tungsten halogen lamp), at normal incidence, in the photon energy range of 0.68-1.54 eV (800-1800 nm), using CM110 monochromator, IR photo-detectors, and an SR-530 lock-in amplifier. The whole setup was automated using the LabView software (Version 8.2). The Hall effect measurement setup was used for the electrical characterization of CIGS thin films using a source meter 2420C (Keithley) and a 6½ digit multimeter 2000 (Keithley). We are using silver-paste, non-rectifying (ohmic) contact. The type of electrical conduction in CIGS thin film was verified using the hot-probe method.

3. RESULTS AND DISCUSSIONS

3.1 Structural Analysis

All annealed and without annealed CIGS thin films show preferred orientation along certain crystallographic planes such as (112), (220) / (204), (312), (400), and (316). This confirms the chalcopyrite phase as per the JCPDS data card 35-1102. Fig. 2a, XRD patterns of CIGS thin films of different thickness grown at 250 ºC substrate temperature, reveals that the thinner CIGS films have an extra minor $Cu_{2-x}Se$ phase ($0 \le x \le 0.2$) (JCPDS 65-2982 and 06-0680) indicated by (200) peak. This is due to the CIGS film is covered with a very thin layer and/or particles of Cu-rich composition [22]. H. Zachmann et al. characterized the CIGS thin film on polyimide substrate. They also observed thin Cu-rich surface layer on CIGS film [23].

Another study by J. Bekker states that before the selenization, there are CuSe and InSe phases present, which were found to be necessary for the incorporation of S into the partly selenized alloy in order to form good quality of absorber layer [24]. As the thickness attains a value close to 0.8 μm, an extra minute $Cu_{2-x}Se$ phase observed, which shows the preferable chalcopyrite phase formation of CIGS thin film. This result corroborates with our previous work [25] based on growth of CIGS thin films.

These CIGS thin films grown at 250 °C of different thicknesses are further annealed at 500 °C by using RTA furnace only for 2 minutes. Rapid annealing treatment improves the quality of the film. Many research groups have checked the effect of thermal annealing of CIGS based thin films grown by different methods [26, 27, 28]. An appreciable improvement is observed after the annealing process, particularly in the (112) tetragonal CIGS phase, which is clearly observed from the XRD spectra shown in Fig. 2b. The thickness of 0.4 and 0.6 μm annealed CIGS film, there is a minor Cu_3Se_2 phase (JCPDS 47-1745) present along with the chalcopyrite CIGS phase, that is indicated as a (101) plane in Fig. 2b. The binary compound products (secondary crystalline phases) are present in the thickness range below 0.6 μm. These binary phases shows detrimental effect on the solar cell performance. When the thickness is raised to above 0.8 μm, Cu_3Se_2 phase disappears while peaks from $CuIn_{0.7}Ga_{0.3}Se_2$ phase, (112) and (220) / (204), start to dominates, as shown in Fig. 2b. This shows, at 1.0 μm thickness, the escalation of a single-phase tetragonal chalcopyrite structure of CIGS.

As per the calculation for the crystalline size, it is observed that, for without annealed CIGS thin film, the crystalline size increases from 42 to 63 nm as the thickness of the CIGS film increases from 0.4 to 1.0 μm. The average lattice parameters $a = 5.655 \pm 0.004$ nm and $c = 11.645 \pm 0.002$ nm are deduced by using Equation 2 [29], matched well with M. Venkatachalam et al. [30]. While annealed CIGS thin films have crystalline size from to 65 to 92 nm as the thickness increases from 0.4 to 1.0 μm and the average lattice parameters are $a = 5.645 \pm 0.003$ nm and $c = 11.628 \pm 0.005$ nm.
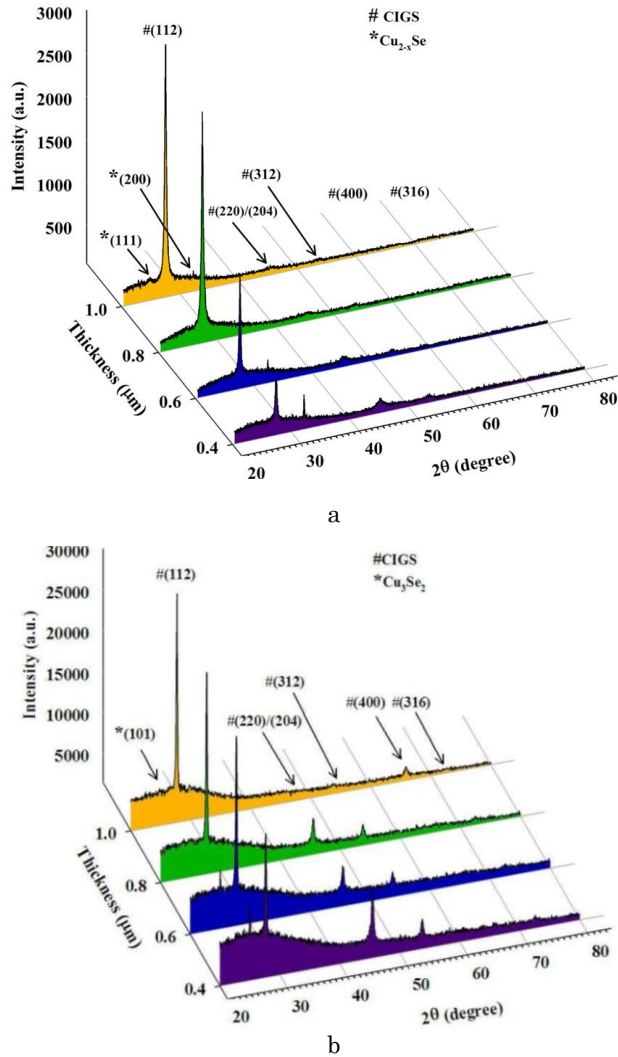
Fig. 2 – XRD of CIGS thin films having a different thickness deposited at 250 ºC substrate temperature (a) and, annealed at 500 ºC (b)

The relation between the lattice parameters and d-spacing for tetragonal system is given by [29],

$$\frac{1}{d^2} = \frac{h^2 + k^2}{a^2} + \frac{1}{c^2} \qquad (1)$$

which may be rewritten in the form,

$$\frac{1}{d^2} = \frac{1}{a^2}\left[(h^2 + k^2) + \frac{1}{(c/a)^2}\right] \qquad (2)$$

3.2 Morphology and Compositional Analysis

Surface morphology, observed using SEM and the compositional analysis by EDS, of annealed CIGS thin films of different thicknesses (0.4 μm to 1 μm) is shown in Fig. 3 and Table 1, respectively. CIS and CIGS based thin films were known for its non-uniform growth due to the non-uniform distribution of constituent elements. In the case of annealed CIGS thin films, the non-uniform distribution of granules and uneven granule size was observed for 0.4 μm thickness. These granules show the Cu-rich composition,

$Cu / (In + Ga) = 2.26$, and due to that overall composition gets disturbed (non-stoichiometry). Surface topography, as shown in Fig. 3, is similar to the results presented by Cunha et al. [31, 32, 33]. The value of $Cu / (In + Ga) = 1.17$ [25] was observed for without annealed 0.8 μm thick CIGS thin films.
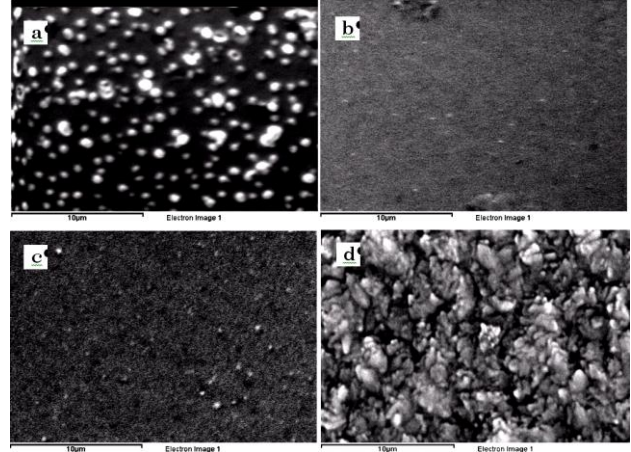

Fig. 3 – SEM images of annealed CIGS thin films of different thicknesses, i.e. 0.4 μm (a), 0.6 μm (b), 0.8 μm (c), and 1.0 μm (d)

Table 1 – Chemical composition of annealed CIGS thin films for different thicknesses from 0.4 to 1.0 μm

Thickness (μm)	Cu (at. %)	In (at. %)	Ga (at. %)	Se (at. %)	O (at. %)
0.4 (particles)	35.98	10.66	5.19	45.97	2.20
0.4 (overall)	39.80	8.86	4.25	44.57	–
0.6	27.53	13.45	5.19	50.63	–
0.8	26.69	17.02	6.50	49.82	–
1.0	24.50	19.07	6.59	49.74	–

We have observed the Cu-rich composition and the nearly smooth film surface up to 0.8 μm thickness. At the thickness, of about 1.0 μm of CIGS thin films, slightly Cu-poor, $Cu / (In + Ga) = 0.95$, composition and rougher surface is observed. Many researchers conclude that, Cu-poor surface is beneficial for improvement of the overall performance of the solar cell [34, 35].

3.3 TEM Analysis

XRD analysis of all CIGS thin films revealed that films had (112) preferred orientation of grains. Among the all CIGS films, 1.0 μm thick annealed films show the preferable structural properties compare to the thinner and unannealed CIGS thin films.

With the XRD measurement the TEM is also carried out for CIGS thin film (1.0 μm thick and RTA processed) in order to confirm the structure of the film which was obtained from the XRD. A small portion of the CIGS film was taken out, by etching in 10 % dilute hydrofluoric (HF) solution, for analyzing the selected-area-diffraction (SAD) pattern which is shown in Fig. 4 (a). The SAD pattern contains continuous sharp rings as expected for polycrystalline films. It can be seen that three major
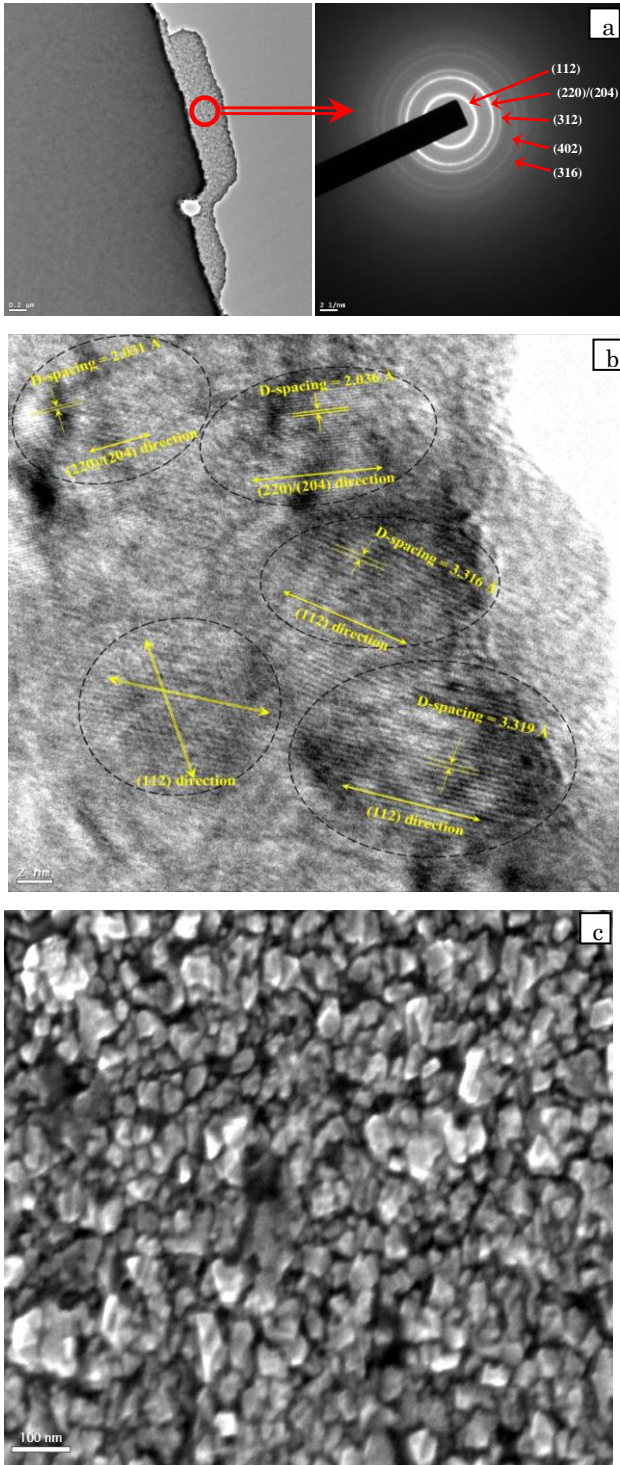
Fig. 4 – SAD pattern (a), high resolution snap-shot (b) and, surface morphology (c) of annealed CIGS thin film

characteristic peaks (112), (220) / (204) and (312) are present in the film. The obtained (hkl) indices of the diffracted rings match with the JCPDS data card 35-1105, for chalcopyrite $Cu(In_{0.7}Ga_{0.3})Se_2$ reflections. Fig. 4b shows a high resolution TEM image that clearly indicates the growth of CIGS polycrystalline material phase having a different d-spacing. The measured d-values is 3.319 ± 0.003 Å and 2.036 ± 0.004 Å, which confirms the growth of grains in (112) and (220) / (204) direction respectively. Fig. 4c shows that the image obtained from

TEM of $1.0\,\mu m$ thick annealed CIGS thin film has a greater resolution compared to that of SEM shown in Fig. 3d. The surface of the CIGS film, as seen from Fig. 4c, demonstrates plenty of compactly packed and faceted grains formed after the RTA process, which implies the appearance of good polycrystalline structure of CIGS films and is consistent with XRD results.

3.4 Optical Analysis

Transmission spectra (normal incidence) and reflection spectra in the wavelength range 800 to 1800 nm, as shown in Fig. 5a were recorded for annealed CIGS thin films of different thicknesses. Lower transmission was observed in the wavelength region of 800 to 1100 nm. Above the 1100 nm wavelength, the transmission increases rapidly. The transmission edge of the spectrum is sharper for films grown at higher thickness, and the maximum level of transmission reached about 65 %. These changes are consistent with the physical properties of the samples observed by the SEM [25]. The improved spectral fringes of reflection spectra indicate the uniform surface morphology of the CIGS annealed thin film of $1.0\,\mu m$ thickness. The average reflection is about 20 % observed from the Fig. 5b. Using the transmission (T) and reflection (R) values at a particular wavelength (λ), the absorption (α) is calculated using the relation [36],

$$\alpha = \frac{1}{t}\left(\ln \frac{(1 - R(\lambda))}{T(\lambda)} \right) \qquad (3)$$

where t is the thickness of the CIGS thin film. By using the absorption values the energy band gap is calculated using the relation,

$$\alpha h\nu = \left[k(h\nu - E_g)^{0.5} \right] \qquad (4)$$

where k is a constant, hu is the photon energy, and E_g is the band gap energy. The plot of $(\alpha h\nu)^2$ versus the photon energy, $h\nu$, for annealed CIGS thin films having different thicknesses is shown in Fig. 6. The low band gap can helps to charge separation, but is detrimental in terms of open circuit voltage; where the wide band gap increases open circuit voltages, it blocks photocurrent collection. The ideal band gap is in the range of 1.10-1.15 eV for CIGS thin film used for solar cell applications.

By extrapolating $(\alpha h\nu)^2$ curves down to a zero level gives an energy band gap value of 1.05 eV for most of the CIGS annealed films, while it is ~ 1.12 eV for without annealed CIGS thin film [25]. The decrease in energy band gap values aster annealing process is consistent with the fact that the crystallinity of the polycrystalline thin films improves on annealing [37].

3.5 Electrical Analysis

The conductivity of an absorber layer plays an important role in the conduction mechanism of solar cells. The change in the resistivity is mainly observed due to micro-structural or surface modification and the thickness variation of CIGS thin film. Variation in the resistivity of the without annealed CIGS films observed as a
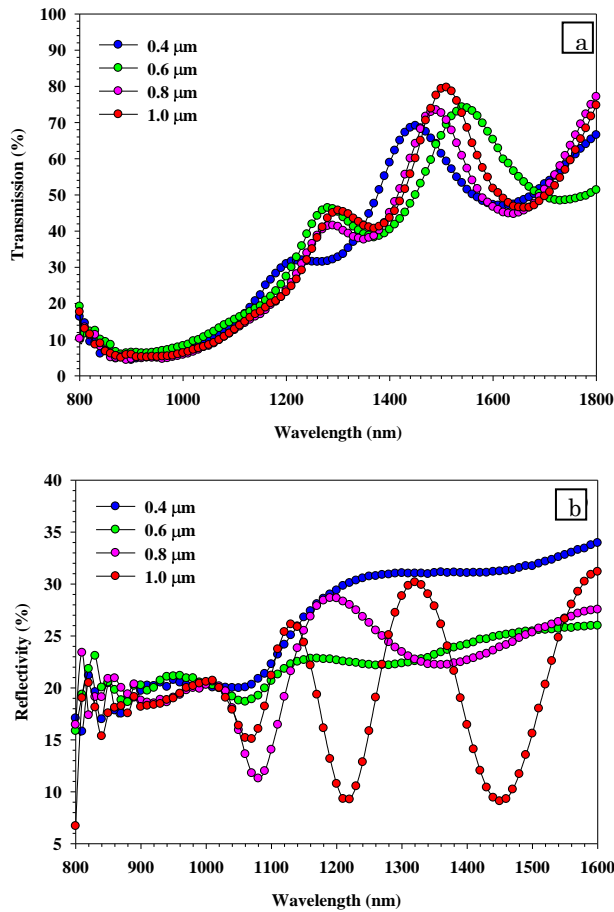
Fig. 5 – Transmission (a), and reflection (b) of annealed CIGS thin films of different thicknesses
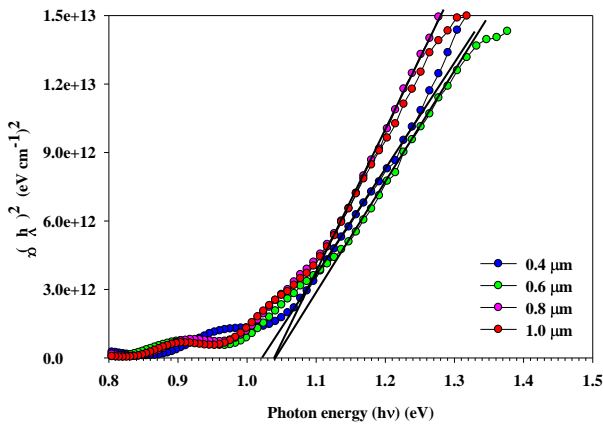

Fig. 6 – Energy band gap of annealed CIGS thin films of different thicknesses

function of film thickness is shown in Fig. 7a. That shows the resistivity was reduced as the thickness increases. With that the improvement in the mobility values (Fig. 7b) were observed due to the improvement in the crystallinity of the film. The observed resistivity for 1.0 μm thickness of CIGS, $4.9 \times 10^2 \, \Omega \cdot$cm, mainly due to the Cu-rich composition of the film surface, that was clearly identified from SEM and EDS analysis [25]. In addition to that the carrier concentration in to the order of $10^{17} \, cm^{-3}$ also supported the Cu-rich composition.
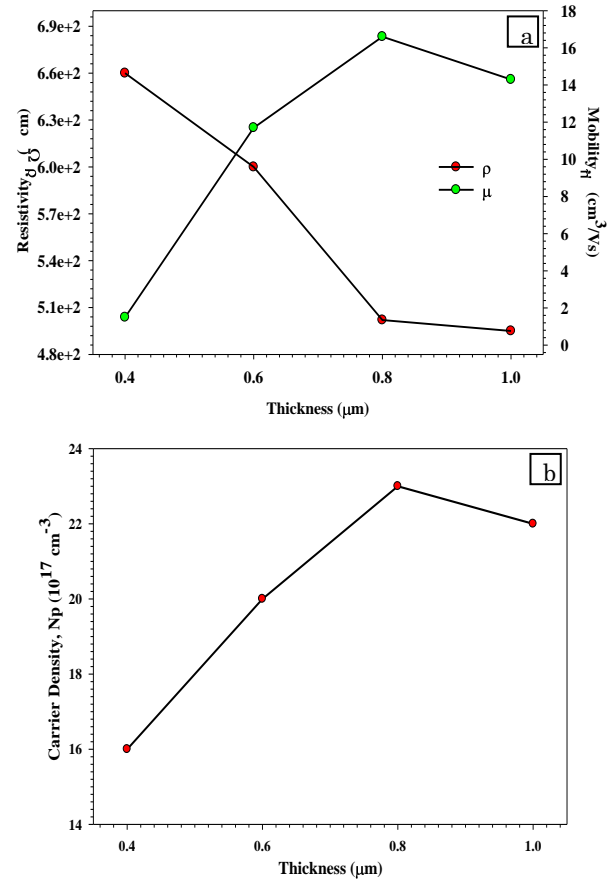

Fig. 7 – Resistivity, ρ, Mobility, μ, (a), and carrier density, N_p, (b) of CIGS thin film of different thicknesses deposited at 250 °C

The variation of resistivity and mobility of annealed CIGS thin film having a different thickness is shown in Fig. 8. The observed significant reduction in the resistivity can be explained from the analysis of the SEM images. At higher substrate temperature, the CIGS thin films experiences a liquid-phase-assisted recrystallization process, which results in the uniform accumulation of the constituent atoms. Therefore, the grain boundaries decreases, and hence the resistivity of the thin film decreases from 6.3×10^2 to $1.9 \times 10^2 \, \Omega \cdot$cm. Improving the grain boundaries, reduce native defect centers and grain boundary defects [38], because of annealing. Therefore the carrier mobility improves. The carrier density for annealed CIGS films reduced from the order of $10^{17} \, cm^{-3}$ (for without annealed) to $10^{16} \, cm^{-3}$. This is in accordance with the improved crystalline structure of CIGS thin film by annealing.

The conductivity type was also measured using hot probe method. All CIGS thin films, annealed and without annealed, exhibit p-type conductivity [39].

3.6 Current-Voltage (I-V) Analysis

An attempt was made to fabricate the hetrojunction of CIGS / CdS to check the performance of the prepared CIGS thin film. The first step was to deposited a 1 μm thick Mo layer on soda lime glass (SLG) substrate, without any intentional substrate heating, by the RF magnetron sputtering [40, 41]. Then, a 1.0 μm
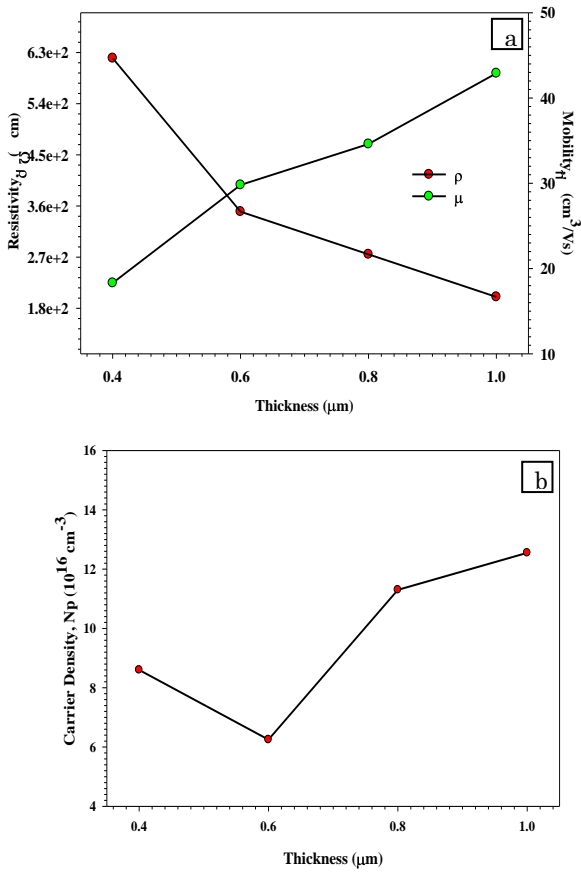
Fig. 8 – Resistivity, ρ, Mobility, μ, (a) and carrier density, N_p, (b) of CIGS thin film of different thicknesses deposited at 250 °C and annealed at 500 °C

thick CIGS layer was deposited on a Mo / SLG substrate by a flash evaporation at the substrate temperature of 250 °C. Prepared CIGS/Mo/SLG structure annealed in RTA furnace. In which the temperature was set to 500 °C for 2 min. The CdS layer was deposited on CIGS film by thermal evaporation [42]. The indium point contact was made on top of CdS layer by thermal
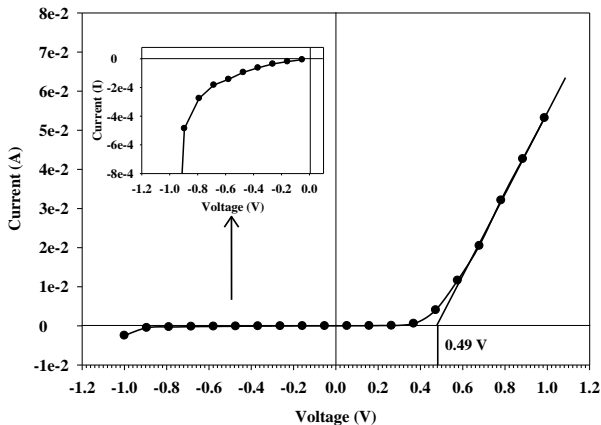

Fig. 9 – Current-Voltage (I-V) characteristics of CIGS / CdS hetero-structure. The inset figure shows the nature of I-V plot in the reverse bias condition

evaporation. Anticipated rectifying behavior was observed from the I-V measurement, shown in Fig. 9. The inset figure shows the I-V characteristics of CIGS / CdS junction in reverse bias condition.

By observing the I-V characteristics, diode voltage threshold of about 0.49 V was observed. Copper migration at the CdS / CIGS inter-face or the edge-face of the junction has been investigated as a possible cause of decrease in threshold of junction [43, 44] compare to the commercial CIGS solar cell. The values of reverse saturation currant and diode ideality factor were about 53 mA/cm² and 1.5, respectively. These preliminary results indicate an evidence of the fact that the CdS buffer layer is suitable for the fabrication of hetero-interface with the CIGS absorber layer. Better results of CIGS / CdS hetero-interface will be expected in future may be by varying the CdS thickness or may be the post heat shock process.

4. CONCLUSIONS

CIGS thin films grown by flash evaporation method by varying the film thickness from 0.4 to 1.0 μm by keeping the substrate temperature at 250 °C. The Influence of rapid thermal annealing clearly show that below 0.6 μm thickness the surface is non-uniform and the Cu-rich composition compare to the thickness of 1.0 μm, which has a Cu-poor composition and packed faceted uniform grains. TEM analysis for the same sample indicates the chalcopyrite structure of CIGS. Transmission and reflection data for CIGS thin films, of different thicknesses, showed the energy band gap value 1.05 eV for most of the annealed CIGS samples. Without annealed CIGS thin films shows the band gap values near to 1.12 eV, mostly due to the Cu-rich composition of CIGS. Because of this the carrier density is in the order of $10^{17}\,cm^{-3}$ and the resistivity is $4.9 \times 10^2\,\Omega\cdot cm$. Rapid thermal annealing improve the crystallization, so the native and grain boundary defects reduce, of CIGS films. That results the decreases in the carrier concentration up to the one order, i.e. $10^{17}\,cm^{-3}$. Higher thickness, 1.0 μm, of CIGS annealed thin films shows the resistivity is $1.9 \times 10^2\,\Omega\cdot cm$, and the carrier concentration is $12.6 \times 10^{17}\,cm^{-3}$. An attempt of preparing PVD grown CIGS / CdS hetero-structure shows the considerable the rectifying behavior from the I-V measurements encourage the detail study of the CIGS / CdS junction in future.

REFERENCES

1. M. Kemell, M. Ritala, M. Leskela, *Crit. Rev. Solid State Mater. Sci.* **30**, 1 (2005).
2. Pyuck-Pa Choi, Oana Cojocaru-Mirédin, Roland Wuerz, Dierk Raabe, *J. Appl. Phys.* **110**, 124513 (2011).
3. P. Jackson, D. Hariskos, E. Lotter, S. Paetel, R. Wuerz, R. Menner, W. Wischmann, M. Powalla, *Prog. Photovolt: Res. Appl.* **19**, 894 (2011).
4. Kihwan Kim, G.M. Hanket, T. Huynh, W.N. Shafarman, *J. Appl. Phys.* **111**, 083710 (2012).
5. M. Marudachalam, R.W. Birkmire, H. Hichri, J.M. Schultz, A. Swartzlander, M.M. Al-Jassim, *J. Appl. Phys.* **82**, 2896 (1997).
6. A. Bouloufa, K. Djessas, D. Todorovic, *Mat. Sci. Semicon. Proc.* **12**, 82 (2009).
7. T.J. Coutts, J.D. Meakin, *Current Topics in Photovoltaics: Vol. 4,* (New York: Academic Press: 1990).
8. S.E. Habas, H.A.S. Platt, M.F.A.M. van Hest, D.S. Ginley, *Chem. Rev.* **110**, 6571 (2010).
9. V. Alberts, M.L. Chenene, *Semicond. Sci. Technol.* **18**, 870 (2003).
10. M. Klenka, O. Schenker, V. Alberts, E. Bucher, *Thin Solid Films* **387**, 47 (2001).
11. M.G. Faraj, K. Ibrahim, A. Salhin, *Int. J. Polym. Mater.* **60**, 817 (2011).
12. Z. Jehl, F. Erfurth, N. Naghavi, L. Lombez, I. Gerard, M. Bouttemy, P. Tran-Van, A. Etcheberry, G. Voorwinden, B. Dimmler, W. Wischmann, M. Powalla, J.F. Guillemoles, D. Lincot, *Thin Solid Films* **519**, 7212 (2011).
13. K. Ramanathan, R. Noufi, B. To, D.L. Young, R. Bhattacharya, M.A. Contreras, R.G. Dhere, G. Teeter, *Conference Record of the 2006 IEEE 4th World Conference on Photovoltaic Energy Conversion,* **1**, 380 (Waikoloa: HI: 2006).
14. O. Lundberg, M. Bodegaard, J. Malmstrom, L. Stolt, *Prog. Photovolt.: Res. Appl.* **11**, 77 (2003).
15. T. Negami, S. Nishiwaki, Y. Hashimoto, N. Kohara, *Proceedings of the 2nd WCPEC*, 1181 (Austria: Vienna:1998).
16. Yuuki Umeno, Tokio Nakada, *3rd World Conference on Photovoltaic Energy Conversion, 1,* 380 (Japan: Osaka: 2003).
17. A. Romeo, M. Terheggen, D. Abou-Ras, D. L. Batzner, F.-J. Haug, M. Kalin, D. Rudmann, A.N. Tiwari, *Prog. Photovolt.: Res. Appl.* **12**, 93 (2004).
18. R. Klenk, T. Walter, H.W. Schock, D. Cahen, *Adv. Mater.* **5**, 114 (1993).
19. Harin S. Ullal, Kenneth Zweibel, Bolko G. von Roedem, *Record of the 28th IEEE Photovoltaic Specialists Conference,* 418 (Alaska: Anchorage: 2000).
20. J.R. Ray, C.J. Panchal, M.S. Desai, *Proceedings of the 54th DAE Solid State Physics Symposium* **54**, 447 (2009).
21. N.M. Shah, J.R. Ray, V.A. Kheraj, M.S. Desai, C.J. Panchal, Bharti Rehani, *J. Mater. Sci.* **44**, 316 (2009).
22. J.R. Tuttle, D.S. Albin, R. Noufi, *Sol. Cells* **30**, 21 (1991).
23. H. Zachmann, S. Heinker, A. Braun, A.V. Mudryi, V.F. Gremenok, A.V. Ivaniukovich, M.V. Yakushev, *Thin Solid Films* **517**, 2209 (2009).
24. J. Bekker, *Sol. Energ. Mat. Sol. C.* **93**, 539 (2009).
25. C.J. Panchal, J.R. Ray, M.S. Desai, Bharati Rehani, *AIP Conf. Proc.* **1451**, 251 (2012).
26. C.J. Hibberd, M. Ganchev, M. Kaelin, S.E. Dann, G. Bilger, H.U. Upadhyaya, A.N. Tiwari, *Thin Solid Films* **517**, 2235 (2009).
27. Erees Queen B. Macabebe, Charles J. Sheppard, Vivian Alberts, E. Ernest van Dyk, *Thin Solid Films* **517**, 2380 (2009).
28. D. Abou-Ras, *Thin Solid Films* **517**, 2218 (2009).
29. B.D. Cullity, *Elements of X-ray diffraction*, (USA, Addison-Wesley Publishing Company, Inc.: 1956).
30. M. Venkatachalam, M.D. Kannan, S. Jayakumar, R. Balasundaraprabhu, N. Muthukumarasamy, *Thin Solid Films* **516**, 6848 (2008).
31. A.F.D. Cunha, F. Kurdesau, D. Rudmann, P.M.P. Salome, *J. Non-Cryst. Solids* **352**, 1976 (2006).
32. A.N. Molin, A.I. Dikusar, G.A. Kiosse, P.A. Petrenko, A.I. Sokolovsky, Yu.G. Saltanovsky, *Thin Solid Films* **237**, 66 (1994).
33. A. Garg, K.S. Balakrisnan, A.C. Rastogi, *J. Electrochem. Soc.* **141**, 1566 (1994).
34. R. Caballero, C. Guille´n, M.T. Gutie´rrez, C.A. Kaufmann, *Prog. Photovolt: Res. Appl.* **14**, 145 (2006).
35. Y.C. Lin, Z.Q. Lin, C.H. Shen, L.Q. Wang, C.T. Ha, Chris Peng, *J. Mater. Sci.: Mater. El.* **23**, 493 (2012).
36. J. Tauc. *Amorphous and Liquid Semiconductors* (New York: Plenum Press: 1974).
37. Hongyong Zhang, Naoto Kusumoto, *United States Patent No. 5352291* (1994).
38. S.B. Zhang, S.-H. Wei, A. Zunger, *Phys. Rev. Lett.* **78**, 4059 (1997).
39. S.A. Dinca, E.A. Schiff, B. Egaas, R. Noufi, D.L. Young, W.N. Shafarman, *Phys. Rev. B* **80**, 235201 (2009).
40. J.R. Ray, N.M. Shah, M.S. Desai, C.J. Panchal, *J. Nano.-Electron. Phys.* **3**, 766 (2011).
41. Cherng-Yuh Su, Kuang-Hsiang Liao, Cheng-Tang Pan, Pei-Wen Peng, *Thin Solid Films* **520**, 5936 (2012).
42. N.M. Shah, J.R. Ray, M.S. Desai, C.J. Panchal, *J. Optoelectron. Adv. M.* **12**, 2052 (2010).
43. J.F. Guillemoles, L. Kronik, D. Cahen, U. Rau, A. Jasenek, H.W. Schock, *J. Phys. Chem. B* **104**, 4849 (2000).
    T. Yanagisawa, T. Kojima, T. Koyanagi, *Microelectron. Reliab.* **44**, 229 (2004).